High q-state clock spin glasses in three dimensions and the Lyapunov exponents of chaotic phases and chaotic phase boundaries

Efe Ilker[1] and A. Nihat Berker[1,2]

[1]*Faculty of Engineering and Natural Sciences, Sabancı University, Tuzla 34956, Istanbul, Turkey*

[2]*Department of Physics, Massachusetts Institute of Technology, Cambridge, Massachusetts 02139, USA*

(Received 13 January 2013; published 11 March 2013)

Spin-glass phases and phase transitions for q-state clock models and their $q \to \infty$ limit the XY model, in spatial dimension $d = 3$, are studied by a detailed renormalization-group study that is exact for the $d = 3$ hierarchical lattice and approximate for the cubic lattice. In addition to the now well-established chaotic rescaling behavior of the spin-glass phase, each of the two types of spin-glass phase boundaries displays, under renormalization-group trajectories, their own distinctive chaotic behavior. These chaotic renormalization-group trajectories subdivide into two categories, namely as strong-coupling chaos (in the spin-glass phase and, distinctly, on the spin-glass–ferromagnetic phase boundary) and as intermediate-coupling chaos (on the spin-glass–paramagnetic phase boundary). We thus characterize each different phase and phase boundary exhibiting chaos by its distinct Lyapunov exponent, which we calculate. We show that, under renormalization group, chaotic trajectories and fixed distributions are mechanistically and quantitatively equivalent. The phase diagrams of arbitrary even q-state clock spin-glass models in $d = 3$ are calculated. These models, for all non-infinite q, have a finite-temperature spin-glass phase. Furthermore, the spin-glass phases exhibit a universal ordering behavior, independent of q. The spin-glass phases and the spin-glass–paramagnetic phase boundaries exhibit universal fixed distributions, chaotic trajectories and Lyapunov exponents. In the XY model limit, our calculations indicate a zero-temperature spin-glass phase.

DOI: 10.1103/PhysRevE.87.032124 PACS number(s): 75.10.Nr, 05.10.Cc, 64.60.De, 75.50.Lk

I. INTRODUCTION

Spin-glass phases, with randomly frozen local order [1] and chaotic behavior under scale change [2–4], reflecting the effects of frozen interaction disorder, competition, and frustration, remain a uniquely fascinating and broadly relevant subject of statistical mechanics and condensed matter physics. However, the large and richly complex amount of theoretical knowledge produced on spin glasses has been overwhelmingly derived from Ising, i.e., $s_i = \pm 1$, spin models [5].

By contrast, we present here a detailed renormalization-group study of spin-glass phases and phase transitions, for q-state clock models and their $q \to \infty$ limit the XY model, in spatial dimension $d = 3$. We note that, in addition to the now well-established chaotic behavior of the spin-glass phase [2–4,6–25], each of the two types of spin-glass phase boundaries displays, under renormalization-group trajectories, their own distinctive chaotic behavior. We see that these chaotic renormalization-group trajectories subdivide into two categories, namely as strong-coupling chaos (in the spin-glass phase and, distinctly, on the spin-glass–ferromagnetic phase boundary) and as intermediate-coupling chaos (on the spin-glass–paramagnetic phase boundary). We thus quantitatively characterize each different phase and phase boundary exhibiting chaos by its distinct Lyapunov exponent as used in the general chaotic studies literature [26,27], which we calculate. We show that, under renormalization-group, chaotic trajectories and fixed distributions are mechanistically and quantitatively equivalent.

We calculate and display the phase diagrams of arbitrary even q-state clock spin-glass models in $d = 3$. These models, for any non-infinite q, have a finite-temperature spin-glass phase. Furthermore, we find that the spin-glass phases exhibit a universal ordering behavior, independent of q. The spin-glass phases and the spin-glass–paramagnetic phase boundary exhibit universal fixed distributions, chaotic trajectories and Lyapunov exponents. In the $d = 3$ XY model limit, our calculations indicate a zero-temperature spin-glass phase.

II. THE q-STATE CLOCK SPIN-GLASS MODEL AND THE RENORMALIZATION-GROUP METHOD

The q-state clock models are composed of unit spins that are confined to a plane and that can only point along q angularly equidistant directions. Accordingly, the q-state clock spin-glass model is defined by the Hamiltonian

$$-\beta\mathcal{H} = \sum_{\langle ij \rangle} J_{ij}\vec{s}_i \cdot \vec{s}_j = \sum_{\langle ij \rangle} J_{ij}\cos(\theta_i - \theta_j), \qquad (1)$$

where $\beta = 1/k_BT$, at site i the spin angle θ_i takes on the values $(2\pi/q)\sigma_i$ with $\sigma_i = 0,1,2,\ldots,q-1$, and $\langle ij \rangle$ denotes that the sum runs over all nearest-neighbor pairs of sites. The bond strengths J_{ij} are $+J > 0$ (ferromagnetic) with probability $1-p$ and $-J$ (antiferromagnetic) with probability p. This model becomes the Ising model for $q = 2$ and the XY model for $q \to \infty$.

The q-state clock spin-glass model, in $d = 3$ dimensions, is readily solved by a renormalization-group method that is approximate on the cubic lattice [28,29] and simultaneously exact on the hierarchical lattice [30–34]. Under rescaling, for $q > 4$, the form of the interaction as given in the rightmost side of Eq. (1) is not conserved and one must therefore express the Hamiltonian more generally, as

$$-\beta\mathcal{H} = \sum_{\langle ij \rangle} V(\theta_i - \theta_j). \qquad (2)$$

Thus, the renormalization-group flows, for even q, are the flows of $1+q/2$ interaction constants. With no loss of generality, the maximum value of $V(\theta_i-\theta_j)$ is set to zero.

The renormalization-group transformation, for spatial dimensions $d=3$ and length rescaling factor $b=3$ (necessary for treating the ferromagnetic and antiferromagnetic correlations on equal footing), is achieved by a sequence of bond moving

$$V_{bm}(\theta_1-\theta_2)+G_{12}=\sum_{n=1}^{b^{d-1}}V_n(\theta_1-\theta_2) \tag{3}$$

and decimation

$$e^{V_{\rm dec}(\theta_1-\theta_4)+G_{14}}=\sum_{\theta_2,\theta_3}e^{V_1(\theta_1-\theta_2)+V_2(\theta_2-\theta_3)+V_3(\theta_3-\theta_4)}, \tag{4}$$

where the constants G_{ij} are fixed by the requirement that the maximum value of $V(\theta_i-\theta_j)$ is zero.

The starting bimodal quenched probability distribution of the interactions, characterized by p and described above, is also not conserved under rescaling. The renormalized quenched probability distribution of the interactions is obtained by the convolution [35]

$$P'(V'(\theta_{i'j'}))=\int\left[\prod_{ij}^{i'j'}dV(\theta_{ij})P(V(\theta_{ij}))\right]\delta(V'(\theta_{i'j'})-R(\{V(\theta_{ij})\})), \tag{5}$$

where $R(\{V(\theta_{ij})\})$ represents the bond moving and decimation given in Eqs. (3) and (4). For numerical practicality, the bond moving and decimation of Eqs. (3) and (4) are achieved by a sequence of pairwise combination of interactions, as shown in Fig. 1(c), each pairwise combination leading to an intermediate probability distribution resulting from a pairwise convolution as in Eq. (5). We effect this procedure numerically, by generating 5 000 interactions that embody the quenched probability distribution resulting from each pairwise combination. Each of the generated 5 000 interactions is determined by $1+q/2$ interaction constants. At each pairwise convolution as in Eq. (5), 5 000 randomly chosen pairs are matched by Eq. (3) or Eq. (4), and a new set of 5 000 is produced. We have checked that our results are insensitive to further increasing the number 5 000. Furthermore, our calculated phase diagrams exactly match, for $q=2$, the results in Refs. [36–39] which are numerically exact by the use of the histogram representation of the quenched probability distribution.

The different thermodynamic phases of the model are identified by the different asymptotic renormalization-group flows of the quenched probability distributions. For all renormalization-group flows, inside the phases and on the phase boundaries, Eq. (5) is iterated until asymptotic behavior is reached, meaning that we are studying an effectively infinite hierarchical lattice. Thus, we are able to calculate phase diagrams for any number of clock states q. Our results are obtained by averaging over 30 to 50 different realizations of the initial $\pm J\cos(\theta_i-\theta_j)$ distribution into the 5 000 initial interactions. In this study, we consider even values of q and the calculated phase diagrams are symmetric around $p=0.5$ with the antiferromagnetic phase replacing the ferromagnetic phase, so that only the $p=0$ to 0.5 halves are shown below. If q is odd, the system does not have sublattice spin-reversal symmetry, which leads to asymmetric phase diagrams.

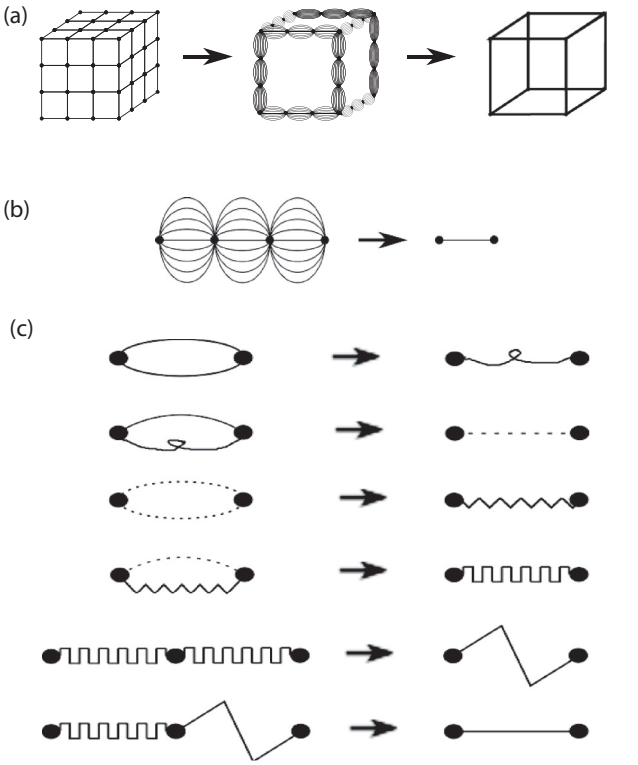

FIG. 1. (a) Migdal-Kadanoff approximate renormalization-group transformation for the $d=3$ cubic lattice with the length-rescaling factor of $b=3$. Bond-moving is followed by decimation. (b) Exact renormalization-group transformation for the equivalent $d=3$ hierarchical lattice with the length-rescaling factor of $b=3$. (c) Pairwise applications of the quenched probability convolution of Eq. (5), leading to the exact transformation in (b).

III. CALCULATED PHASE DIAGRAMS FOR $d=3$ q-STATE CLOCK AND XY SPIN GLASSES

Our calculated phase diagrams for the $q=2,4,6,12$ clock spin-glass models are shown together in Fig. 2. The phase diagram for the XY limit, namely $q\to\infty$, is also shown in Fig. 2, calculated here with $q=360$ clock states. In this limit, the spin-glass phase disappears at zero temperature, whereas the phase boundary between the ferromagnetic and paramagnetic phases numerically stabilizes, on the scale of the figure, for $q\gtrsim 6$. The paramagnetic–ferromagnetic–spin-glass reentrance as temperature is lowered, previously seen [36,40] for $q=2$, namely the Ising case, is also seen here for the other q. As q is increased, it is found that the spin-glass phase retreats to lower temperatures while further protruding into the ferromagnetic phase.

The calculated phase diagrams for the high-q models, $q=12,18,36,360$, are shown in Fig. 3. As q is increased, the trend mentioned above, of the spin-glass phase retreating to lower temperatures while further protruding into the ferromagnetic phase, is also seen here. Furthermore, two

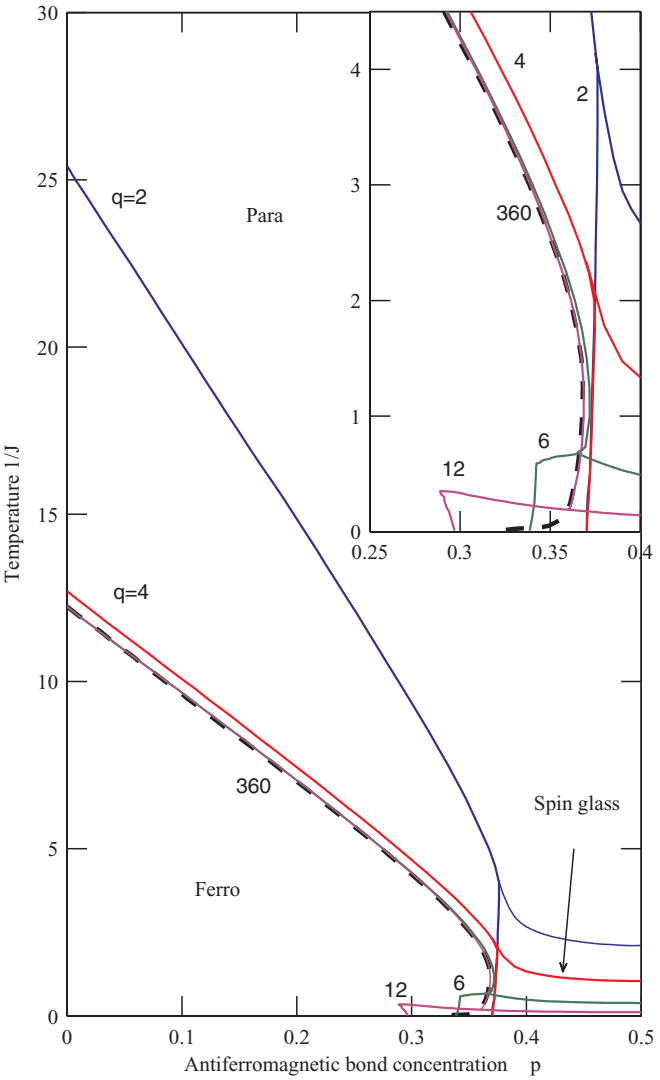

FIG. 2. (Color online) Calculated phase diagrams of the $q = 2,4,6,12$ clock spin-glass models in $d = 3$ dimensions. The phase diagram for the XY limit, namely $q \to \infty$, is also shown, by the dashed curve, calculated here with $q = 360$ clock states. As q is increased, it is found that the spin-glass phase retreats to lower temperatures while further protruding into the ferromagnetic phase. In the XY limit, the spin-glass phase disappears at zero temperature (see Fig. 4 below), as the phase boundary between the remaining ferromagnetic and paramagnetic phases numerically stabilizes, on the scale of the figure, for $q \gtrsim 6$.

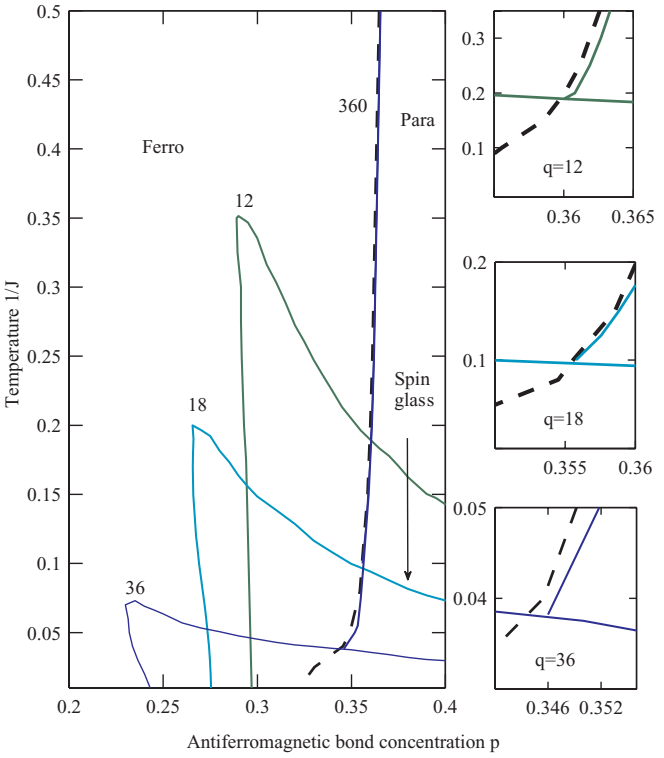

FIG. 3. (Color online) Phase diagrams of the $q = 12,18,36$ clock spin-glass models in $d = 3$ dimensions. Two new phenomena are simultaneously detected here: (1) double reentrance: paramagnetic–ferromagnetic–spin-glass–ferromagnetic as temperature is lowered, (2) lateral reentrance: ferromagnetic–spin-glass–ferromagnetic–paramagnetic as p is increased. The XY limit is given, calculated here with $q = 360$ clock states, by the dashed curve. The panels on the right show the region of the multicritical point, where the three phase boundary lines meet, for each q case along with the ferromagnetic-paramagnetic phase boundary of the XY limit.

new phenomena are simultaneously detected here: (1) double reentrance, namely paramagnetic–ferromagnetic–spin-glass–ferromagnetic phases as temperature is lowered; (2) lateral reentrance, namely ferromagnetic–spin-glass–ferromagnetic–paramagnetic phases as p is increased. Multiple reentrances have previously been seen in liquid crystal systems [41–43].

The (slow) disappearance of the q-state clock spin-glass phase is shown in Fig. 4, where the calculated spin-glass transition temperatures at $p = 0.5$ are shown as a function of q, up to very large values of $q = 720$. The slow decay of the transition temperature suggests that a zero-temperature spin-glass phase [44] exists in the $q \to \infty$, namely XY model limit, in agreement with the previous Monte Carlo study of Ref. [19].

IV. STABLE FIXED DISTRIBUTION AND CHAOTIC RENORMALIZATION-GROUP TRAJECTORY OF CLOCK SPIN-GLASS PHASES

A. Stable fixed distribution

For the spin-glass phase of the Ising model ($q = 2$), under repeated renormalization-group transformations, the quenched probability distribution of the interactions across the system becomes symmetric in ferromagnetic ($J_{ij} > 0$) and antiferromagnetic ($J_{ij} < 0$) couplings, with the average magnitude of either type of interaction equal and diverging to infinity [36].

For the spin-glass phases of all q-state clock models, we find that under repeated renormalization-group transformations, the interaction values $V_{ij}(\theta)$ divide into two groups: $\theta = 2\pi n/q$ and $\theta = 2\pi m/q$, where n is an even integer, $n = 0, 2, 4, \ldots, q-2$, and m is an odd integer, $m = 1, 3, 5, \ldots, q-1$. The asymptotic renormalized quenched distribution of the interactions is symmetric, with interactions equal within each group mentioned above, but at each location overwhelmingly

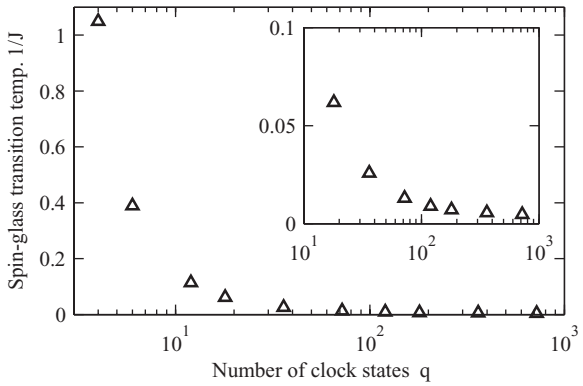

FIG. 4. The calculated transition temperatures between the spin-glass phase and the paramagnetic phase, at $p = 0.5$, as a function of q, up to very large values of $q = 720$. Note the logarithmic scale of the horizontal axes. The slow decay of the transition temperature suggests that a zero-temperature spin-glass phase exists in the $(q \to \infty)$ XY model limit.

favoring one or the other of the two groups. Thus, the interaction difference between the two groups,

$$\frac{1}{q/2}\sum_{n=0,2,\ldots}^{q-2} V_{ij}(2\pi n/q) - \frac{1}{q/2}\sum_{m=1,3,\ldots}^{q-1} V_{ij}(2\pi m/q) \equiv U_{ij}, \tag{6}$$

after many renormalization-group transformations, is randomly and equally distributed as positive or negative in our sampling of 5 000 interactions, which represent the distribution of interactions spatially across the system, with the average magnitude of either type of interaction equal and diverging to infinity as $b^{0.24n}$, where n is the number of iterations. This asymptotic fixed distribution, namely the sink of the spin-glass phase, is shown in Fig. 5. Note that this asymptotic behavior is also consistent with the behavior of the Ising spin-glass phase (U reduces to J for the Ising case), recalled at the beginning of this section. This behavior leaves the system asymptotically frustrated.

B. Chaotic renormalization-group trajectory

The fact that the Ising spin-glass phase is characterized by the chaotic rescaling behavior of the interactions [2–4], and therefore of the correlations [23], is now well established [2–4,6–25] and is also seen here for the spin-glass phases of the q-state clock models in $d = 3$, as shown in Fig. 5. As with the Ising model [7], we have here a strong-coupling chaotic behavior: The values of the interaction difference U_{ij} obtained by successive renormalization-group transformations at any specific location, divided by the average magnitude $\langle|U|\rangle$ across the system, fall into a chaotic band. Thus, the $U_{ij}/\langle|U|\rangle$ values are sampled within the band as shown in Fig. 5. The average magnitude $\langle|U|\rangle$ diverges to infinity under repeated renormalization-group transformations, as $b^{0.24n}$, where n is the number of iterations.

We thus realize that the spin-glass phases can be characterized by the Lyapunov exponent of general chaotic behavior [26,27]. The positivity of the Lyapunov exponent measures the

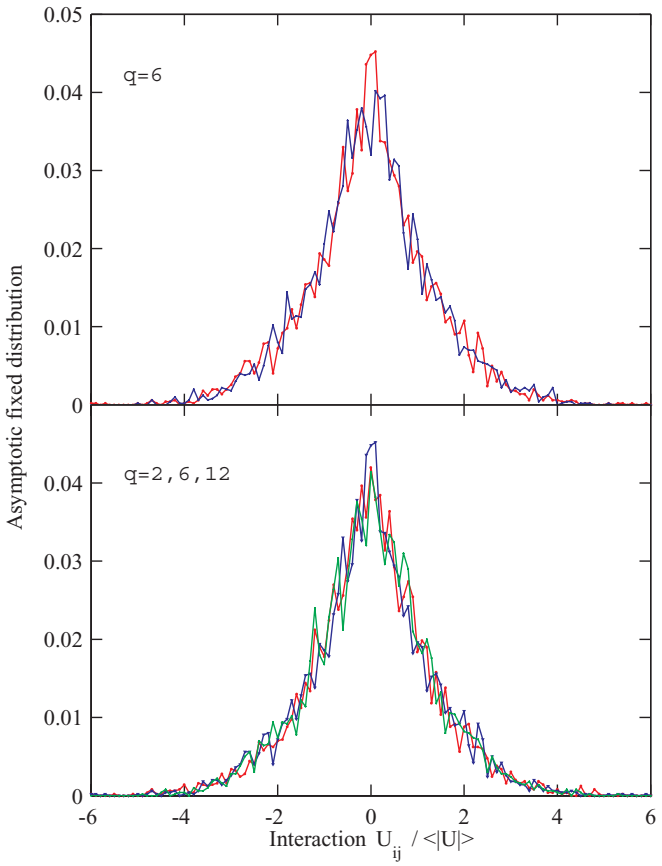

FIG. 5. (Color online) Asymptotic fixed distribution, under renormalization-group transformations, of the interactions in the spin-glass phase, namely the renormalization-group sink of the spin-glass phase. Note that these are strong-coupling distributions, as the average interaction strength $\langle|U|\rangle$ diverges to infinity under the renormalization-group transformations. The divergence of $\langle|U|\rangle$ is as $b^{0.24n}$, where n is the number of iterations. Top: For the $q = 6$-state clock model in $d = 3$, for a trajectory starting in the spin-glass phase at $p = 0.5$ and temperature $1/J = 0.05$, the distributions after 20 and 21 renormalization-group steps are shown. It is seen that these two distributions coincide, signifying a fixed distribution. Bottom: Asymptotic fixed distributions of the spin-glass phases for the $q = 2$ (Ising), 6,12-state clock models in $d = 3$. These distributions are reached after 20 renormalization-group steps, starting at $p = 0.5$ and temperature $1/J = 0.05$. Note that the spin-glass sink fixed distributions for different values of q coincide. The Lyapunov exponent is $\lambda = 1.93$ for the single, universal distribution that is illustrated in this figure.

strength of the chaos [26,27] and was also used in the previous spin-glass study of Ref. [23]. The calculation of the Lyapunov exponent is applied here to the chaotic renormalization-group trajectory at any specific location in the lattice,

$$\lambda = \lim_{n\to\infty} \frac{1}{n}\sum_{k=0}^{n-1} \ln\left|\frac{dx_{k+1}}{dx_k}\right|, \tag{7}$$

where $x_k = U_{ij}/\langle|U|\rangle$ at step k of the renormalization-group trajectory. The sum in Eq. (7) is to be taken within the asymptotic chaotic band. Thus, we throw out the first 100 renormalization-group iterations to eliminate the points outside of, but leading to the chaotic band. Subsequently, typically

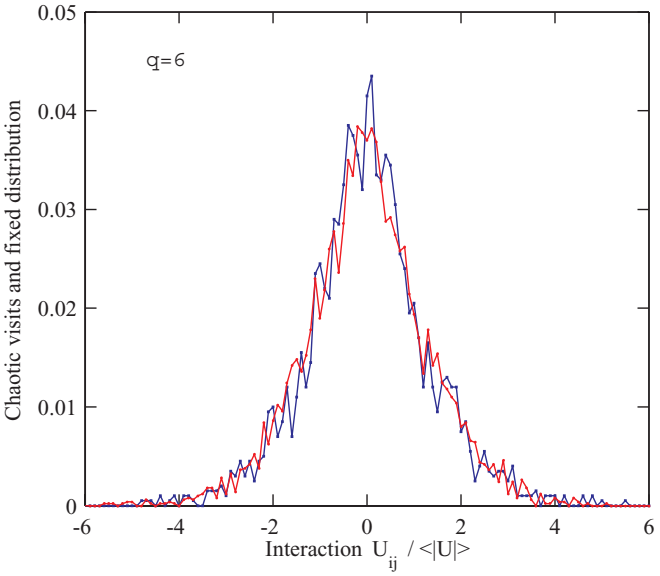

FIG. 6. (Color online) Comparison, showing the coincidence, of the chaotic visits of the consecutively renormalized interactions at a given position of the system (for 2 000 renormalization-group iterations) and of the asymptotic distribution of the interactions across the system at a given renormalization-group step, for the spin-glass phase. The Lyapunov exponent is $\lambda = 1.93$. Identical asymptotic behavior occurs for all q-state clock spin-glass phases, as shown in Fig. 5. The divergence of $\langle |U| \rangle$ is as $b^{0.24n}$, where n is the number of iterations.

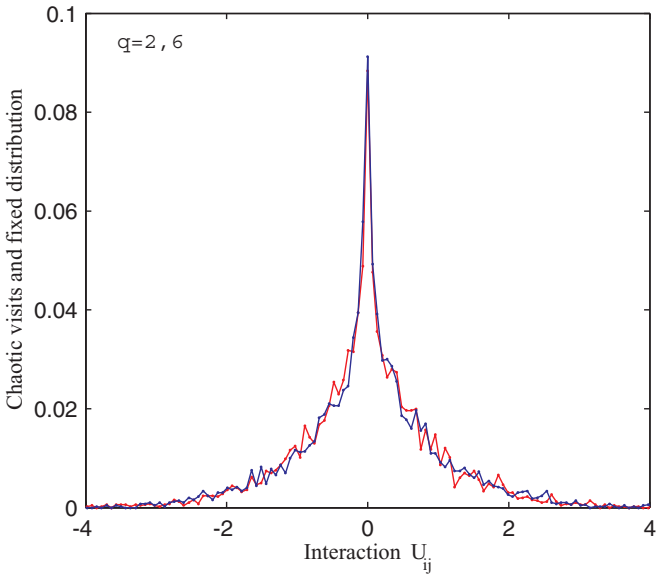

FIG. 7. (Color online) The fixed distribution and, equivalently, chaotic renormalization-group trajectory onto which the phase boundary between the spin-glass and paramagnetic phases renormalizes, for the $q = 2$- and $q = 6$-state clock models in $d = 3$. The Lyapunov exponent is $\lambda = 1.35$. Identical asymptotic behavior occurs for all q. Note that the chaotic behavior and fixed distribution are at intermediate coupling strength, with $\langle |U| \rangle = 0.686$ for all q.

using 2 000 renormalization-group iterations in the sum in Eq. (7) assures the convergence of the Lyapunov exponent value. We have calculated the Lyapunov exponent $\lambda = 1.93$ for the clock spin-glass phases of $q = 2, 6, 12$ and presumably for the clock spin-glass phases of all q, which is to be expected since all q spin-glass phases renormalize to the same chaotic band, as seen in Fig. 5.

C. Equivalence of the chaotic renormalization-group trajectory and the quenched probability fixed distribution

The distributions of the interaction difference U_{ij} values shown in Figs. 5 and 6, respectively obtained as the spatial distribution across the system after many renormalization-group transformations and the values obtained by successive renormalization-group transformations at a specific location in the system, are in fact identical, as seen in Fig. 6. Thus, it is understood that the asymptotic fixed distribution is realized, after a given number of renormalization-group transformations, by the interactions at different locations being at different points of the same chaotic trajectory.

V. UNSTABLE FIXED DISTRIBUTIONS AND CHAOTIC RENORMALIZATION-GROUP TRAJECTORIES OF THE CLOCK SPIN-GLASS–PARAMAGNETIC AND SPIN-GLASS–FERROMAGNETIC BOUNDARIES

We find that the points on the various spin-glass phase boundaries also renormalize to a fixed distribution of the quenched interactions across the system and, equivalently, to a chaotic renormalization-group trajectory of the interaction at any single location in the lattice. The difference between the asymptotic rescaling behaviors inside the spin-glass phase and on the spin-glass phase boundaries is that, under rescaling transformations, the fixed distribution and the chaotic trajectory are reached in a stable manner, with respect to initial conditions, for the spin-glass phase and are conversely unstable for the spin-glass phase boundaries. The ferromagnetic-paramagnetic phase boundary renormalizes to the pure ferromagnetic system, where an unstable fixed point determines the critical exponent, differently for each q.

A. Spin-glass–paramagnetic phase boundary

The phase boundary between the spin-glass and paramagnetic phases renormalizes to the fixed distribution and chaotic renormalization-group trajectory shown in Fig. 7. The interaction grouping, under rescaling, described before Eq. (6) also happens. However, this behavior here occurs at finite coupling $\langle |U| \rangle = 0.686$ for all q, in contrast to the asymptotic behaviors of the spin-glass phase (given above) and of the spin-glass–ferromagnetic phase boundary (given below), which occur at strong coupling $\langle |U| \rangle \to \infty$.

B. Spin-glass–ferromagnetic phase boundary

The phase boundary between the spin-glass and ferromagnetic phases renormalizes to a fixed distribution and chaotic renormalization-group trajectory at strong coupling $\langle |U| \rangle \to \infty$. The interaction grouping, under rescaling, described before Eq. (6) does not happen. Thus, the interaction $V(\theta)$ as a function of θ has $1 + q/2$ different values. The

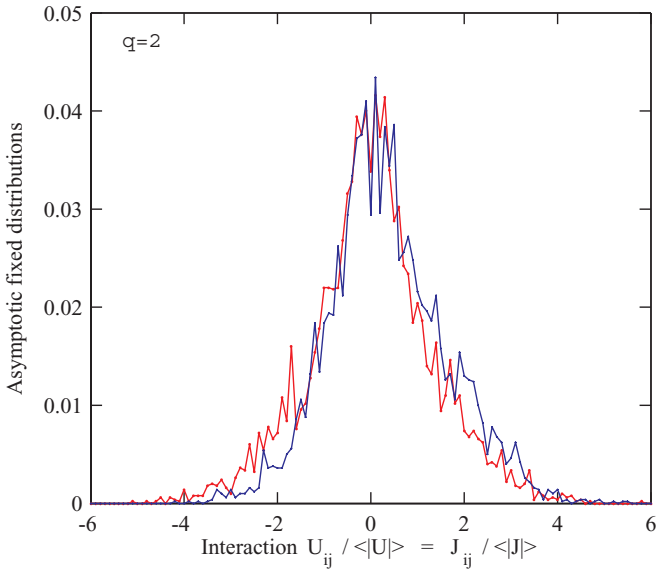

FIG. 8. (Color online) Two different, non-coinciding strong-coupling fixed distributions: The fixed distribution and, equivalently, chaotic renormalization-group trajectory onto which the spin-glass–ferromagnetic phase boundary of the $q = 2$-state model in $d = 3$ renormalizes. For comparison and distinction, the asymptotic fixed distribution and chaotic renormalization-group trajectory of the corresponding spin-glass phase is also shown. The latter curve is symmetric around $U_{ij}/\langle|U|\rangle = 0$, whereas the former curve is noticeably displaced towards positive (ferromagnetic) interaction values. Note that these are strong-coupling distributions and are therefore shown as a fraction of the diverging $\langle|U|\rangle$. The divergence of $\langle|U|\rangle$ is as $b^{0.46n}$ and $b^{0.24n}$, where n is the number of iterations, respectively for the phase boundary and phase sink cases. Thus, even small shifts in the shown curves signify large differences in the interaction values. The Lyapunov exponents are $\lambda = 1.69$ and 1.93, respectively, for the phase boundary and phase sink cases. For $q = 2$, the form of the interaction in Eq. (1) is conserved under renormalization, which is reflected in the horizontal axis label here.

asymptotic fixed distribution for $q = 2$ is shown in Fig. 8 and is characterized by the Lyapunov exponent $\lambda = 1.69$. The divergence of $\langle|U|\rangle$ is as $b^{0.46n}$, where n is the number of iterations.

The asymptotic fixed distribution for $q = 6$ is shown in Fig. 9. The full fixed distribution has the form $P(\{V(0), V(60), V(120), V(180)\})$, as a coupled function of its arguments. The dominant configurations of this fixed distribution are shown in Table I. The system remains frustrated at all length scales.

TABLE I. Dominant potentials in the asymptotic fixed distribution of the phase boundary between the spin-glass and ferromagnetic phases of the $q = 6$ clock model in $d = 3$. Thus, the system remains frustrated at all length scales.

Weight in fixed dist.	$e^{V(0)}$	$e^{V(60)}$	$e^{V(120)}$	$e^{V(180)}$
0.4802	1	0	0	0
0.3951	0	1	0	0
0.1139	1	0	1/2	0
0.0108	0	1	0	2/3

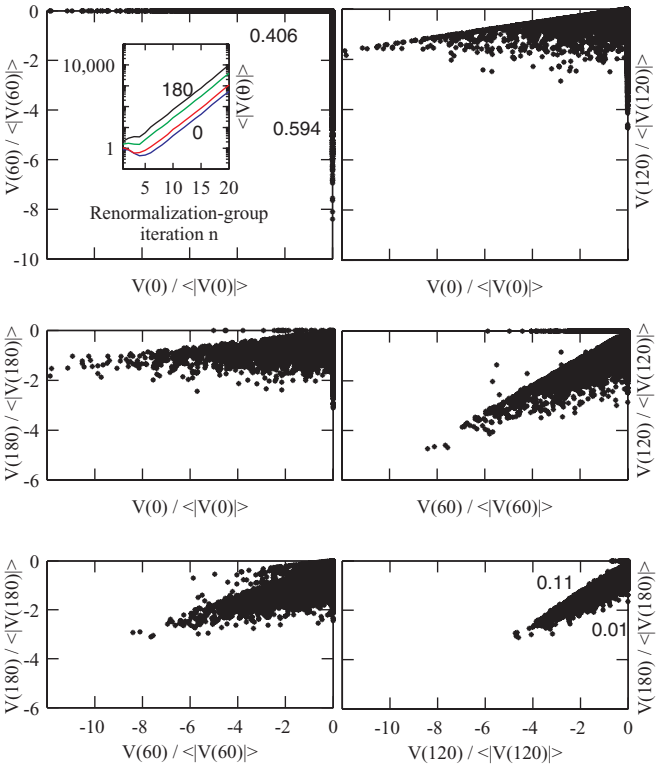

FIG. 9. (Color online) The fixed distribution and, equivalently, chaotic renormalization-group trajectory onto which the spin-glass–ferromagnetic phase boundary of the $q = 6$-state clock model in $d = 3$ renormalizes. The coupled distributions of the interactions $V(\theta)/\langle|V(\theta)|\rangle$ are shown, while next to each axis, the fraction of points on the axis are given. The full fixed distribution has the form $P(\{V(0), V(60), V(120), V(180)\})$, as a coupled function of its arguments. This is a strong-coupling behavior: The inset in the upper left panel shows, with the logarithmic vertical scale, the diverging $\langle|V(\theta)|\rangle$ as a function of renormalization-group iteration n, the consecutive curves being for $\theta = 180, 120, 60, 0$. It is seen that, for all θ, $\langle|V(\theta)|\rangle$ diverges as $b^{0.46n}$, where n is the number of iterations.

VI. CONCLUSION

We have calculated, from renormalization-group theory, the phase diagrams of arbitrary even q-state clock spin-glass models in $d = 3$. These models, for all non-infinite q, have a finite-temperature spin-glass phase, exhibiting a universal ordering behavior, independent of q. In addition to the chaotic rescaling behavior of the spin-glass phase, each of the two types of spin-glass phase boundaries displays, under renormalization-group trajectories, their own distinctive chaotic behavior, subdividing into two categories: strong-coupling chaos, in the spin-glass phase and distinctly on the spin-glass–ferromagnetic phase boundary, and intermediate-coupling chaos, on the spin-glass–paramagnetic phase boundary. We uniquely characterize each different phase and phase boundary exhibiting chaos by its distinct Lyapunov exponent from general chaos studies, which we calculate. We demonstrate that, under renormalization-

group, chaotic trajectories and fixed distributions are mechanistically and quantitatively equivalent. The spin-glass phases and the spin-glass–paramagnetic phase boundaries exhibit universal fixed distributions, chaotic trajectories and Lyapunov exponents. In the XY model limit, our calculations indicate a zero-temperature spin-glass phase.

ACKNOWLEDGMENTS

Support by the Alexander von Humboldt Foundation, the Scientific and Technological Research Council of Turkey (TÜBITAK), and the Academy of Sciences of Turkey (TÜBA) is gratefully acknowledged.

[1] H. Nishimori, *Statistical Physics of Spin Glasses and Information Processing* (Oxford University Press, Oxford, 2001).
[2] S. R. McKay, A. N. Berker, and S. Kirkpatrick, Phys. Rev. Lett. **48**, 767 (1982).
[3] S. R. McKay, A. N. Berker, and S. Kirkpatrick, J. Appl. Phys. **53**, 7974 (1982).
[4] A. N. Berker and S. R. McKay, J. Stat. Phys. **36**, 787 (1984).
[5] For two applications to quantum Heisenberg spin glasses, see C. N. Kaplan and A. N. Berker, Phys. Rev. Lett. **100**, 027204 (2008); P. C. Menezes and A. Theumann, Phys. Rev. B **78**, 054444 (2008).
[6] A. J. Bray and M. A. Moore, Phys. Rev. Lett. **58**, 57 (1987).
[7] E. J. Hartford and S. R. McKay, J. Appl. Phys. **70**, 6068 (1991).
[8] M. Nifle and H. J. Hilhorst, Phys. Rev. Lett. **68**, 2992 (1992).
[9] M. Nifle and H. J. Hilhorst, Physica A **194**, 462 (1993).
[10] M. Cieplak, M. S. Li, and J. R. Banavar, Phys. Rev. B **47**, 5022 (1993).
[11] F. Krzakala, Europhys. Lett. **66**, 847 (2004).
[12] F. Krzakala and J. P. Bouchaud, Europhys. Lett. **72**, 472 (2005).
[13] M. Sasaki, K. Hukushima, H. Yoshino, and H. Takayama, Phys. Rev. Lett. **95**, 267203 (2005).
[14] J. Lukic, E. Marinari, O. C. Martin, and S. Sabatini, J. Stat. Mech.: Theory Exp. (2006) L10001.
[15] P. Le Doussal, Phys. Rev. Lett. **96**, 235702 (2006).
[16] T. Rizzo and H. Yoshino, Phys. Rev. B **73**, 064416 (2006).
[17] H. G. Katzgraber and F. Krzakala, Phys. Rev. Lett. **98**, 017201 (2007).
[18] H. Yoshino and T. Rizzo, Phys. Rev. B **77**, 104429 (2008).
[19] J. H. Pixley and A. P. Young, Phys. Rev. B **78**, 014419 (2008).
[20] T. Aspelmeier, Phys. Rev. Lett. **100**, 117205 (2008).
[21] T. Aspelmeier, J. Phys. A **41**, 205005 (2008).
[22] T. Mora and L. Zdeborova, J. Stat. Phys. **131**, 1121 (2008).
[23] N. Aral and A. N. Berker, Phys. Rev. B **79**, 014434 (2009).
[24] Q. H. Chen, Phys. Rev. B **80**, 144420 (2009).
[25] T. Jörg and F. Krzakala, J. Stat. Mech.: Theory Exp. (**2012**) L01001.
[26] P. Collet and J.-P. Eckmann, *Iterated Maps on the Interval as Dynamical Systems* (Birkhäuser, Boston, 1980).
[27] R. C. Hilborn, *Chaos and Nonlinear Dynamics*, 2nd ed. (Oxford University Press, New York, 2003).
[28] A. A. Migdal, Zh. Eksp. Teor. Fiz. **69**, 1457 (1975) [Sov. Phys. JETP **42**, 743 (1976)].
[29] L. P. Kadanoff, Ann. Phys. (NY) **100**, 359 (1976).
[30] A. N. Berker and S. Ostlund, J. Phys. C **12**, 4961 (1979).
[31] R. B. Griffiths and M. Kaufman, Phys. Rev. B **26**, 5022R (1982).
[32] M. Kaufman and R. B. Griffiths, Phys. Rev. B **30**, 244 (1984).
[33] S. R. McKay and A. N. Berker, Phys. Rev. B **29**, 1315 (1984).
[34] M. Hinczewski and A. N. Berker, Phys. Rev. E **73**, 066126 (2006).
[35] D. Andelman and A. N. Berker, Phys. Rev. B **29**, 2630 (1984).
[36] G. Migliorini and A. N. Berker, Phys. Rev. B. **57**, 426 (1998).
[37] M. Hinczewski and A. N. Berker, Phys. Rev. B **72**, 144402 (2005).
[38] C. Güven, A. N. Berker, M. Hinczewski, and H. Nishimori, Phys. Rev. E **77**, 061110 (2008).
[39] G. Gülpınar and A. N. Berker, Phys. Rev. E **79**, 021110 (2009).
[40] S. B. Roy and M. K. Chattopadhyay, Phys. Rev. B **79**, 052407 (2009).
[41] J. O. Indekeu and A. N. Berker, Physica A (Utrecht) **140**, 368 (1986).
[42] R. R. Netz and A. N. Berker, Phys. Rev. Lett. **68**, 333 (1992).
[43] M. G. Mazza and M. Schoen, Int. J. Mol. Sci. **12**, 5352 (2011).
[44] G. Grinstein, A. N. Berker, J. Chalupa, and M. Wortis, Phys. Rev. Lett. **36**, 1508 (1976).